Low Computational Enhancement of STFT-Based Parameter Estimation

Binhee Kim, *Member, IEEE*, Seung-Hyun Kong, *Member, IEEE*, and Suil Kim

***Abstract*—Short-time Fourier transform (STFT) is one of the most widely used tools to analyze frequency and phase of local sections of time-varying signals using a time window function. Since the fixed window size of STFT causes limitation in time-frequency representation (TFR), adaptive STFT (ASTFT) techniques have been studied to adjust the window size depending on the local signal characteristics. However, ASTFT techniques suffer from heavy computational complexity in general. In this paper, we propose low computational enhanced temporal and spectral parameter estimation techniques for STFT output of radar signals; forward and backward STFT enhancement techniques. The proposed forward STFT enhancement technique is to enhance the spectral resolution of a received radar signal by multiple times using a number of successive STFT outputs without applying additional STFT with wider time window. On the other hand, the proposed backward STFT enhancement technique is to improve the temporal resolution of a received radar signal using an STFT output with a wide time window, without applying multiple STFTs with smaller time window. The performance of the proposed techniques are theoretically analyzed, and the advantage of the proposed techniques to the conventional techniques in terms of computational complexity is demonstrated with numerous simulations.**

***Index Terms*—Short-time Fourier transform (STFT), temporal and spectral resolution, time–frequency representation.**

I. Introduction

TIME-FREQUENCY representation (TFR) is a widely used tool to characterize signals with time-varying frequency such as speech, radar, and biomedical signals [1]–[6], and the temporal and spectral resolutions are important criteria to adequately characterize the signal. However, according to the Heisenberg uncertainty principle [1], the product of the temporal resolution and the spectral resolution should be larger than $1/(4\pi)$, known as the Heisenberg box. Due to this principle, increase of temporal resolution induces the decrease of spectral resolution, and vice versa. Therefore, there have been studies to find an appropriate temporal and spectral resolutions to represent the signals of interests.

Short-time Fourier transform (STFT) is one of the classical techniques to obtain the TFR [7] of time-varying signals, where STFT utilizes a time window function of fixed size to choose local input signal before applying the Fourier transform (FT), and, because of the fixed size time window, STFT may suffer from poor temporal-spectral resolution. To adjust the time-frequency resolution appropriately to time-varying signals, a number of adaptive STFT (ASTFT) techniques have been introduced in the literature [8]–[11], most of which can be classified into two groups; one is the concentration measure (CM)-based, and the other is chirp-rate (CR)-based [7]. In the CM-based ASTFT, the effects of certain parameter variations on the energy concentration of the input signal is examined in the time-frequency domain to find the optimum parameter value, yielding the highest energy concentration, which is used to perform STFT [12], [13]. Therefore, the CM-based ASTFT can produce useful results, however, the process to find the optimum parameter value is computationally expensive. The CR-based ASTFT utilizes wavelet transform (WT) to obtain the first derivative of the instantaneous frequency (IF) which is then used to determine the window size of the STFT so that the signal inside the chosen time window is quasi-stationary [14], [15].

While the CR-based ASTFT has less computational complexity than the CM-based ASTFT, we still use STFT as a principle TFR analysis tool in many applications due to the computational cost of the CR-based ASTFT. In applications such as radar signal processing, received or received-and-dechirped signals are sparse and often appear around a certain frequency component in the frequency-domain, in which case it is possible to reduce computational complexity to estimate the spectral information of the signal with much finer resolution than the CR-based ASTFT. Instead of employing an additional complex algorithm to determine the time window size to enhance the parameter estimation of radar signals with finer resolution as in the conventional ASTFT techniques, we propose two low computational techniques to enhance the parameter estimation using the STFT output(s). The proposed forward STFT enhancement technique can estimate the spectral information of the radar signal with N_2 times finer spectral resolution than that available from N_2 successive STFT outputs with low spectral resolution. Similarly, the proposed backward STFT enhancement technique can obtain the temporal information of the radar signal with a temporal resolution T/N_2 directly utilizing an STFT output that has a temporal resolution T. The performance of the proposed

Manuscript received January 29, 2015; revised May 09, 2015; accepted July 23, 2015. Date of publication August 06, 2015; date of current version November 17, 2015. This work was supported by the Electronic Warfare Research Center (EWRC) grant funded by the Agency for Defense Development (ADD). The guest editor coordinating the review of this manuscript and approving it for publication was Prof. Xiaopeng Yang. *(Corresponding author: S.-H. Kong.)*

B. Kim and S.-H. Kong are with the Korea Advanced Institute of Science and Technology (KAIST), Daejeon 305-701, Korea (e-mail: vini@kaist.ac.kr; skong@kaist.ac.kr).

S. Kim is with the Agency of Defense Development, Daejeon 305-600, Korea (e-mail: sikim777@add.re.kr).

Color versions of one or more of the figures in this paper are available online at http://ieeexplore.ieee.org.

Digital Object Identifier 10.1109/JSTSP.2015.2465310

techniques in radar signal processing is theoretically analyzed, and the computational advantage of the proposed techniques is demonstrated in comparison to the conventional techniques.

The rest of this paper is organized as follows. We introduce the principles of STFT briefly and key notations used in this paper in Section II. The proposed low computational enhancement of STFT-based parameter estimation techniques are introduced in Section III. The performance of the proposed techniques is analyzed in terms of error and computational complexity in Section IV, and the performance simulation results of the proposed techniques are compared to the conventional techniques in Section V. And finally, Section VI draws the conclusion of this paper.

II. Short-Time Fourier Transform

Short-time Fourier transform (STFT) is widely used to find the time-frequency representations of local sections of time-varying signals using a time window function. The N_1-point STFT of the input signal $r[n]$ is represented as [3]

$$X_1[k_1, m_1] = \sum_{n_1=0}^{N_1-1} r[n_1 + N_1 m_1] e^{-j2\pi n_1 k_1/N_1}, \quad (1)$$

where $n = n_1 + N_1 m_1$, N_1 is the total number of samples within the time window (i.e., window size) used in the STFT, $n_1 \in \{0, \ldots, N_1 - 1\}$ is the index of samples within a time window, $m_1 \in \{0, \ldots, M-1\}$ is the index of a time window, M is the total number of consecutive time windows, and k_1 is the frequency index. Fig. 1(a) illustrates the temporal and spectral resolution related to the STFT process in (1). As shown, the temporal width of a block represents the size (i.e., width) of the time window, and the height of a block is the corresponding spectral resolution that can be expressed as

$$\Delta f_1 = \frac{1}{N_1 T_s}, \quad (2)$$

where T_s is the sampling interval. When STFT is used for N_2 times finer spectral resolution than X_1 (1), $N_1 N_2$-point STFT of the input signal should be applied as

$$X_2[k_2, m_2] = \sum_{n=0}^{N_1 N_2 - 1} r[n_1 + N_1 n_2 + N_1 N_2 m_2] \times e^{-j2\pi(n_1 + N_1 n_2)k_2/(N_1 N_2)}, \quad (3)$$

where $k_2 = k_0 + N_2 k_1$, and k_0 denotes the index of a finer spectral component generated by N_2 times wider time window than the STFT in (1). Moreover, $m_1 = n_2 + N_2 m_2$, $M = N_2 N_3$, $n = n_1 + N_1 n_2 + N_1 N_2 m_2$, where $n_2 \in \{0, \ldots, N_2 - 1\}$ denotes the index of a longer time interval generated by the N_2 times wider time window, $m_2 \in \{0, \ldots, N_3 - 1\}$ is the index of a successive time window for $N_1 N_2$-point STFT. Therefore, the finer spectral resolution for X_2 is

$$\Delta f_2 = \frac{1}{N_1 N_2 T_s}. \quad (4)$$

The temporal and spectral resolutions of (3) are shown in Fig. 1(b). As shown in Fig. 1(a) and Fig. 1(b), $X_2[k_2, m_2]$ has N_2 times coarser temporal resolution than $X_1[k_1, m_1]$, but $X_2[k_2, m_2]$ has N_2 times finer spectral resolution than $X_1[k_1, m_1]$.

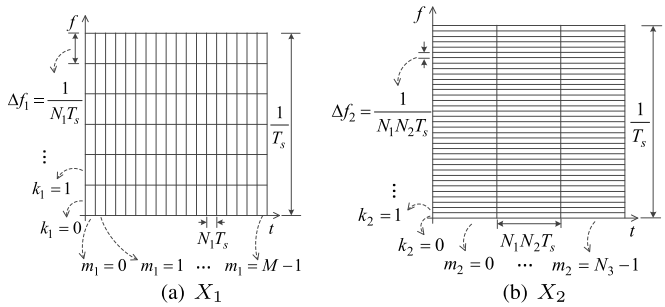

Fig. 1. Time-frequency representation of X_1 and X_2.

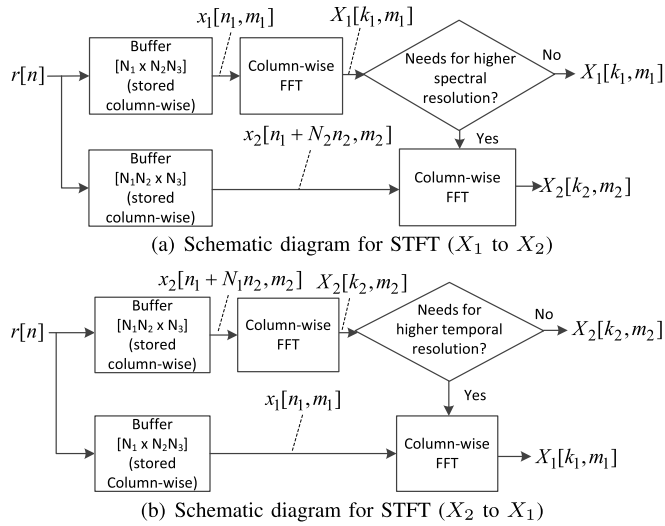

Fig. 2. Schematic diagrams for the conventional STFT.

In general, the spectral resolution available from $X_2[k_2, m_2]$ is not directly obtainable from $X_1[k_1, m_1]$. In other words, when N_2 times finer spectral resolution than $X_1[k_1, m_1]$ is needed, $X_2[k_2, m_2]$ should be computed with a separate STFT. This process is illustrated in Fig. 2(a). First, time-domain signal samples, $r[n]$, are stored column-wise in the $[N_1 \times N_2 N_3]$ array buffer to build $x_1[n_1, m_1]$, and column-wise fast Fourier transform (FFT) [16] is applied to $x_1[n_1, m_1]$ to obtain $X_1[k_1, m_1]$. When N_2 times finer spectral resolution than $X_1[k_1, m_1]$ is required, $N_1 N_2$-point column-wise FFT is applied to the time-domain samples, $x_2[n_1 + N_1 n_2, m_2]$, stored in the $[N_1 N_2 \times N_3]$ array buffer.

In an opposite example shown in Fig. 2(b), even if $X_2[k_2, m_2]$ is obtained from $r[n]$, $X_1[k_1, m_1]$ should be directly calculated from $r[n]$ again to obtain N_2 times finer temporal resolution than $X_2[k_2, m_2]$. First, the time-domain signal samples $r[n]$ are stored column-wise in the $[N_1 N_2 \times N_3]$ array buffer to build $x_2[n_1 + N_1 n_2, m_2]$, and $N_1 N_2$-point column-wise FFT is applied to $x_2[n_1 + N_1 n_2, m_2]$ to obtain $X_2[k_2, m_2]$. When N_2 times finer temporal resolution than $X_2[k_2, m_2]$ is needed, N_1-point column-wise FFT is applied to time-domain signal samples $r[n]$ stored column-wise in the $[N_1 \times N_2 N_3]$ array buffer.

As a result, separate STFTs should be performed for the same signal to achieve desired temporal and spectral resolutions, where the STFT output with different temporal and spectral resolutions is not utilizable. In the next section, for signals

with concentrated spectral components such as radar signals, we introduce low computational techniques to estimate the signal parameters with finer temporal and spectral resolution utilizing the already obtained STFT output(s) that has(have) lower temporal or spectral resolution, respectively.

III. Low Computational High-Resolution STFT

In this section, forward STFT and backward STFT enhancement techniques are introduced in detail. The proposed technique to improve the spectral resolution of $X_1[k_1, m_1]$ to that of $X_2[k_2, m_2]$ is denoted as 'forward STFT enhancement technique', and the proposed technique to increase the temporal resolution of $X_2[k_2, m_2]$ to that of $X_1[k_1, m_1]$ is denoted as 'backward STFT enhancement technique'.

A. Proposed Forward STFT Enhancement Technique

The proposed forward STFT enhancement technique is to obtain $N_1(>1)$ times finer spectral information available from the STFT output X_2 utilizing only $N_1(>1)$ consecutive STFT outputs, X_1's, which have the same low spectral resolution.

The N_1N_2-point STFT $X_2[k_2, m_2]$ of the signal $x_2[n_1 + N_1n_2, m_2]$ can be rearranged in terms of the N_1-point STFT as

$$\begin{aligned} X_2[k_2, m_2] &= \sum_{n_2=0}^{N_2-1}\sum_{n_1=0}^{N_1-1} x_2[n_1 + N_1n_2, m_2] \\ &\quad \times e^{-j2\pi(k_0+N_2k_1)(n_1+N_1n_2)/(N_1N_2)} \qquad (5a) \\ &= \sum_{n_2=0}^{N_2-1}\sum_{n_1=0}^{N_1-1} x_2[n_1 + N_1n_2, m_2] \\ &\quad \times e^{(-j2\pi k_0n_1/(N_1N_2))}e^{-j2\pi k_1n_1/N_1} \\ &\quad \times e^{-j2\pi k_0n_2/N_2}. \qquad (5b) \end{aligned}$$

Note that the expression (5b) is a similar form to the two-dimensional (2D) FFT. In other words, $X_2[k_2, m_2]$ can be seen as the 2D FFT as

$$X_2[k_2, m_2] = \sum_{n_2=0}^{N_2-1}\sum_{n_1=0}^{N_1-1} Q[n_1, k_0]e^{-j2\pi k_1n_1/N_1} \times e^{-j2\pi k_0n_2/N_2} \qquad (6)$$

where

$$Q[n_1, k_0] = x_2[n_1 + N_1n_2, m_2]e^{(-j2\pi k_0n_1/(N_1N_2))}. \qquad (7)$$

To derive the relationship between $X_2[k_2, m_2]$ and $X_1[k_1, m_1]$, we use the multiplication-convolution duality property of the Fourier transform to rearrange (6) as [17]

$$\begin{aligned} &X_2[k_2, m_2] \\ &= X_2[k_0 + N_2k_1, m_2] \qquad (8a) \\ &= \sum_{n_2=0}^{N_2-1}\sum_{n_1=0}^{N_1-1} x_2[n_1 + N_1n_2, m_2]e^{(-j2\pi k_0n_1/(N_1N_2))} \\ &\quad \times e^{-j2\pi k_1n_1/N_1}e^{-j2\pi k_0n_2/N_2} \\ &= \sum_{n_2=0}^{N_2-1}\left[\left(\sum_{n_1=0}^{N_1-1} x_2[n_1 + N_1n_2, m_2]e^{-j2\pi k_1n_1/N_1}\right)\right. \\ &\quad \left.\circledast \left(\sum_{n_1=0}^{N_1-1} e^{(-j2\pi k_0n_1/(N_1N_2))}e^{-j2\pi k_1n_1/N_1}\right)\right] \\ &\quad \times e^{-j2\pi k_0n_2/N_2} \qquad (8b) \\ &= \sum_{n_2=0}^{N_2-1} (X_1[k_1, n_2 + N_2m_2] \circledast H_{12}[k_1, k_0]) \\ &\quad \times e^{-j2\pi k_0n_2/N_2}, \qquad (8c) \end{aligned}$$

where

$$\begin{aligned} H_{12}[k_1, k_0] &= \frac{1 - e^{-j2\pi k_0/N_2}}{1 - e^{-j2\pi(k_0+N_2k_1)/(N_1N_2)}} \qquad (9a) \\ &= \frac{\sin(\pi k_0/N_2)}{\sin\left(\pi(k_0 + N_2k_1)/(N_1N_2)\right)} \\ &\quad \times e^{j\pi((k_0+N_2k_1)/(N_1N_2)-k_0/N_2)} \qquad (9b) \end{aligned}$$

represents a transformation function that transforms X_1 to X_2, and $\circledast$ denotes the circular convolution operator. The (8c) leads us to conclude that $X_2[k_2, m_2]$, whose spectral resolution is N_2 times finer than $X_1[k_1, m_1]$, can be obtained using $X_1[k_1, m_1]$ and $H_{12}[k_1, k_0]$. In (8c), the circular convolution between $X_1[k_1, m_1]$ and $H_{12}[k_1, k_0]$ should be computed first, and FFT is applied along n_2 direction to obtain $X_2[k_2, m_2]$. However, for each k_0 of $X_2[k_0 + N_2k_1, m_2]$, $H_{12}[k_1, k_0]$ becomes a column vector so that the circular convolution between $X_1[k_1, m_1]$ and $H_{12}[k_1, k_0]$ becomes a circular convolution between $X_1[k_1, m_1]$ and a column vector $H_{12}[k_1]|_{k_0}$.

From (9b), it is found that $H_{12}[k_1, k_0]$ becomes a cosecant function of k_1 for a fixed k_0. Therefore, $H_{12}[k_1, k_0]$ has a maximum value when the denominator is an integer multiple of π, and $H_{12}[k_1, k_0]$ becomes a Kronecker delta function when k_0 is an integer multiple of N_2. Using L'Hopital's rule and that $0 \le k_0 < N_2$, we can find

$$|H_{12}[k_1, k_0]| = \begin{cases} N_1, & \text{for } k_0 = k_1 = 0 \\ 0, & \text{for } k_0 = 0,\ k_1 \neq 0 \\ \left|\frac{\sin(\pi k_0/N_2)}{\sin(\pi k_1/N_1 + \pi k_0/(N_1N_2))}\right|, & \text{otherwise} \end{cases} \qquad (10)$$

which is an N_1 times weighted Kronecker delta function for $k_0 = 0$ and is similar to an weighted Kronecker delta function when k_0 is close to 0 or close to N_2. Since the phase change of $H_{12}[k_1, k_0]$ due to the change in k_0, i.e., Δk_0, is found as

$$\angle H_{12}[k_1, \Delta k_0] = e^{j\pi(1/(N_1N_2)-1/N_2)\Delta k_0}, \qquad (11)$$

the difference in k_0 results in a phase difference in $\angle H_{12}[k_1, \Delta k_0]$ from 0 to π. Therefore, since (8c) is a homogeneous system, the phase difference of $X_2[k_2, m_2]$ for neighboring k_0 values depends only on Δk_0.

To verify the mathematical analysis, the normalized magnitudes of $H_{12}[k_1]|_{k_0}$ for $k_0 = (0.1, 0.2, 0.5, 0.6, 0.9, 1)N_2$ are evaluated as an example and shown in Fig. 3. From (9b), the argument of the sin function in the denominator has a phase shift as much as $k_0\pi/(N_1N_2)$, which can be found in Fig. 3, where the maximum peak location shifts by $k_0\pi/(N_1N_2)$. As shown in (9b) and Fig. 3, $H_{12}[k_1, k_0]$ can be approximated by a single Kroneckar delta function for k_0 close to zero or close to N_2,

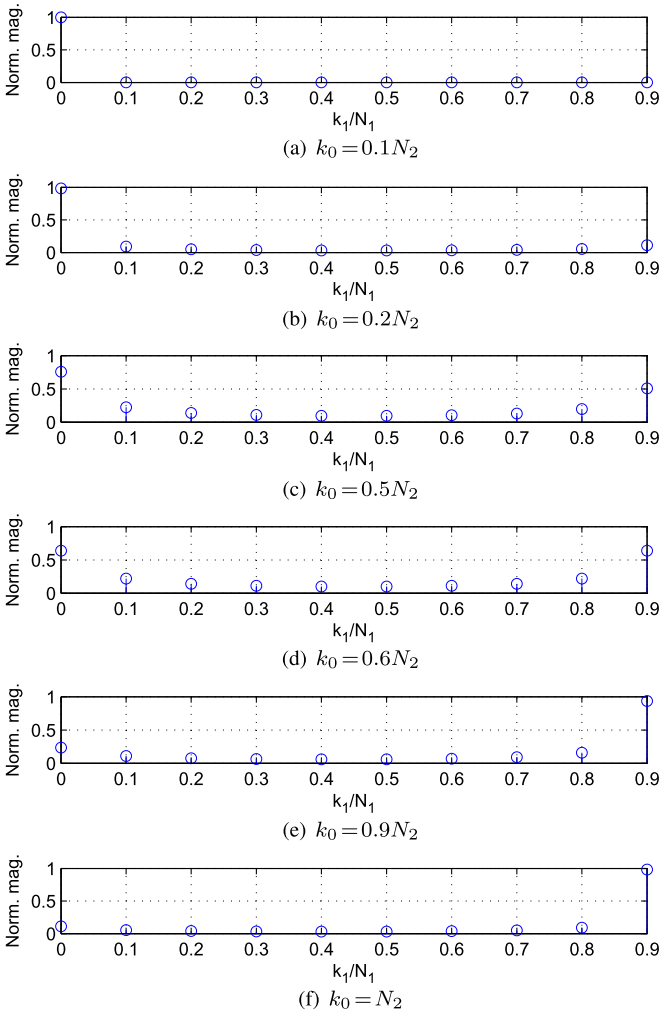

Fig. 3. $H_{12}[k_1, k_0]$ for various values of k_0.

however, $H_{12}[k_1, k_0]$ has multiple non-negligible components and two large peaks when k_0 is not close to zero and N_2. Therefore, for k_0 close to zero or close to N_2, the circular convolution operation of $X_1[k_1, m_1]$ and $H_{12}[k_1, k_0]$ can be replaced with an element shift of $X_1[k_1, m_1]$, and, otherwise, the convolution of $X_1[k_1, m_1]$ and $H_{12}[k_1, k_0]$ should be computed. However, computing the convolution of $X_1[k_1, m_1]$ and $H_{12}[k_1, k_0]$ at every k_0 is computationally inefficient due to the similarity of $H_{12}[k_1, k_0]$ between neighboring k_0's. Therefore, instead of performing the convolution for all values of k_0, some representative values of k_0 can be used to approximate the convolution of $X_1[k_1, m_1]$ and $H_{12}[k_1, k_0]$ to reduce computational complexity. The expression (9a) can be approximated as

$$H_{12}[k_1, k_0] \simeq H_{12}[k_1, \tilde{k}_{0,i}], \quad \text{for } (i-1)\beta N_2 < \left| k_0 - \frac{i\beta N_2}{2} \right| < i\beta N_2 \quad (12)$$

where β is a real number between 0 and 1, $i\beta \leqq 1$, $\tilde{k}_{0,i} = i\beta N_2$ which denotes the representative values of k_0, and $\lfloor 1/\beta \rfloor$ is the number of representative values.

In addition, when evaluating $X_2[k_2, m_2]$ from $X_1[k_1, m_1]$, we can select some k_1 values of interests at which $X_2[k_2, m_2]$ needs to be evaluated for a finer resolution so that the computational complexity can be further reduced. This may be the case when we have a coarse prior knowledge of the spectral components of $r[n]$ via the observation of $X_1[k_1, m_1]$ that provides coarse spectral information. In this paper, we assume that N_I values of k_1 are of interests, where N_I is small.

The error caused by the approximation of $H_{12}[k_1, k_0]$ in (12) is analyzed in Section IV. To find the effect of using the approximated $H_{12}[k_1, k_0]$ in (12) on estimating selected spectral components of $X_2[k_2, m_2]$, we compare $X_{2,E}[k_2, m_2]$, $X_2[k_2, m_2]$, and $X_{2,N}[k_2, m_2]$, where $X_{2,E}[k_2, m_2]$ denotes the low computational estimation of $X_2[k_2, m_2]$ using the approximation of $H_{12}[k_1, k_0]$ in (12), $X_2[k_2, m_2]$ denotes the results of (8c) computed using the $H_{12}[k_1, k_0]$, and $X_{2,N}[k_2, m_2]$ denotes the results of (8c) without $H_{12}[k_1, k_0]$ (i.e., the convolution with $H_{12}[k_1, k_0]$ is neglected by assuming $H_{12}[k_1, k_0] = \delta[k_1, k_0]$). Note that $X_{2,E}[k_2, m_2]$ and $X_2[k_2, m_2]$ are the outputs of the proposed forward STFT enhancement technique, the conventional technique, respectively, and let the method producing $X_{2,N}[k_2, m_2]$ be denoted as the No-H_{12} method in the following analysis.

Schematic diagrams for the No-H_{12} method and the proposed forward STFT enhancement technique are shown in Fig. 4(a) and Fig. 4(b), respectively. In the No-H_{12} method, $r[n]$ is stored column-wise in an $[N_1 \times N_2 N_3]$ array buffer. The stored signal is column-wise FFT'd, and it is tested if the higher spectral resolution is required. For a higher spectral resolution, rows of $X_1[k_1, m_1]$ are selected for the spectral components of interests, where higher spectral resolution is required, and N_2-point row-wise FFT is performed for the selected rows (i.e., k_1's) of interest. In the proposed forward STFT enhancement technique, $r[n]$ is stored column-wise in an $[N_1 \times N_2 N_3]$ array buffer, and the stored signal is column-wise FFT'd. When higher spectral resolution is needed for the spectral components (i.e., k_1's) of interest, column-wise circular convolution between $X_1[k_1, m_1]$ and $H_{12}[k_1, \tilde{k}_{0,i}]$ are performed. Denoting $X_{2,E}^{(i)}$ as the $X_{2,E}$ computed using $H_{12}[k_1, \tilde{k}_{0,i}]$, $X_{2,E}^{(i)}$ is expressed with the N_2-point row-wise FFT for each k_1 of interests as

$$X_{2,E}^{(i)}[k_0 + N_2 k_1, m_2] = \sum_{n_2=0}^{N_2-1} \left(X_1[k_1, n_2 + N_2 m_2] \circledast H_{12}[k_1, \tilde{k}_{0,i}] \right) e^{-j2\pi k_0 n_2 / N_2}, \quad \text{for } (i-1)\beta N_2 < \left| k_0 - \frac{i\beta N_2}{2} \right| < i\beta N_2. \quad (13)$$

The relationship between $X_{2,E}^{(i)}$ and $X_{2,E}$ is found as

$$X_{2,E}\left[(i-1)\beta N_2 + \mathrm{mod}(k_0, \beta N_2) + N_2 k_1, m_2\right] = X_{2,E}^{(i)}[k_0 + N_2 k_1, m_2]. \quad (14)$$

The performance of the No-H_{12} method and the proposed forward STFT enhancement technique is briefly compared in Fig. 5. In the simulation, signals consisted of two sinusoidal components at $f_1 = -200$ kHz and $f_2 = 50$ kHz are sampled at $f_s = 1$ MHz and STFT'd to obtain X_1 for $N_1 = 10$ as shown in Fig. 5(a). From X_1, we compute X_2, $X_{2,N}$, and $X_{2,E}$ as shown

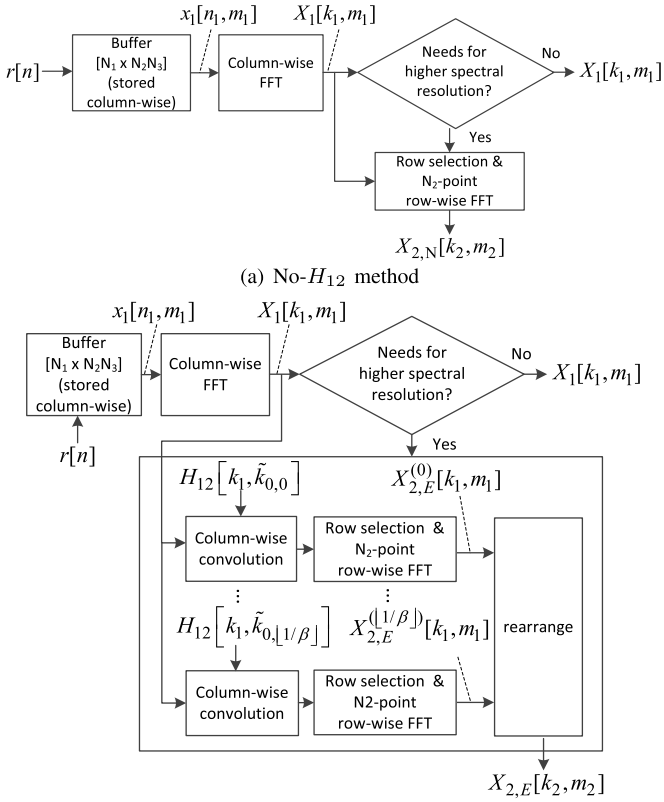

Fig. 4. Schematic diagrams of STFT methods for spectral resolution enhancement. (a) No-H_{12} method; (b) proposed forward STFT enhancement technique.

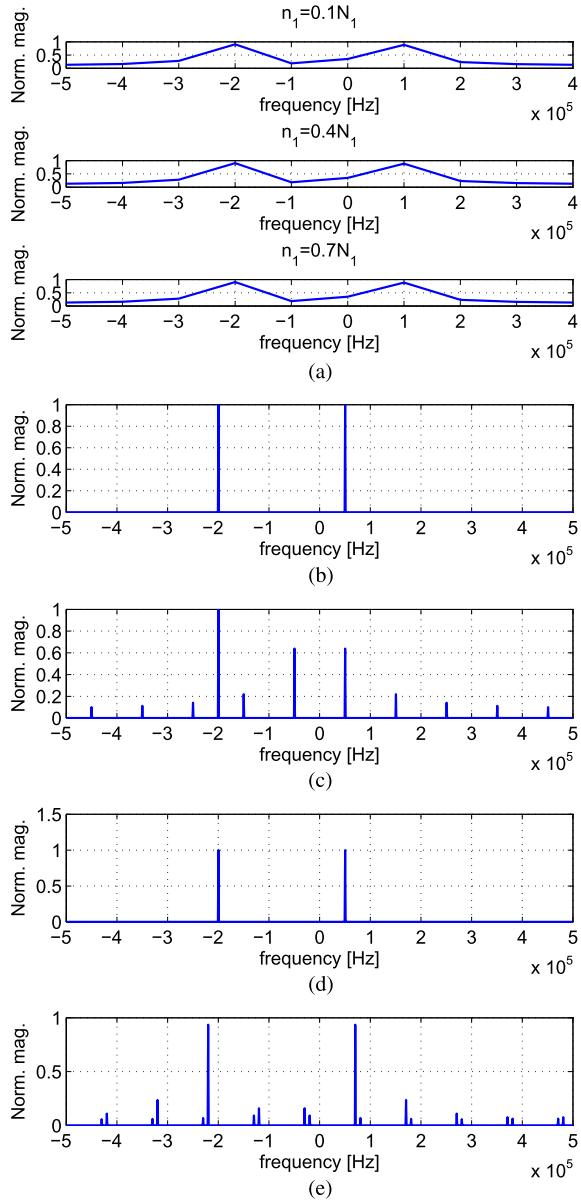

Fig. 5. Example of X_2 obtained from X_1. (a) X_1 with respect to n_2 for $N_1 = 10$, $N_2 = 100$, $f_1 = -200$ kHz, and $f_2 = 50$ kHz; (b) X_2 for $N_1 = 10$, $N_2 = 100$, $f_1 = -200$ kHz, and $f_2 = 50$ kHz; (c) $X_{2,N}$ for $N_1 = 10$, $N_2 = 100$, $f_1 = -200$ kHz, and $f_2 = 50$ kHz; (d) $X_{2,E}$ for $N_1 = 10$, $N_2 = 100$, $f_1 = -200$ kHz, and $f_2 = 50$ kHz; (e) $X_{2,E}$ for $N_1 = 10$, $N_2 = 100$, $f_1 = -220$ kHz, and $f_2 = 70$ kHz.

in Fig. 5(b), Fig. 5(c), and Fig. 5(d), respectively. In Fig. 5(e), we show another example of $X_{2,E}$ for a signal of two sinusoidal components at $f_1 = -220$ kHz and $f_2 = 70$ kHz, where small spectral components at frequencies other than f_1 and f_2 appear due to the approximation of $H_{12}[k_1, k_0]$ in (12). Note that the approximation in (12) causes an error when $k_0 \neq \tilde{k}_{0,i}$, which means that the final approximation error (i.e., $|X_2 - X_{2,E}|$) occurs when the input signal includes frequencies not in multiple of $\beta f_s/N_1$. Therefore, we expect smaller final approximation error for small f_s and large N_1. Overall, the dominant spectral components obtained with the proposed forward STFT enhancement technique shows a good match to the intact X_2. In contrast, the $X_{2,N}$ in Fig. 5(c) has many false peaks and one of the false peak is a dominant spectral component.

B. Proposed Backward STFT Enhancement Technique

In general, an STFT output producing fine spectral resolution cannot have a fine temporal resolution due to the Heisenberg uncertainty principle. The proposed backward STFT enhancement technique is to estimate temporal information available from the N_1-point STFT output X_1 using the N_1N_2-point STFT output X_2. In practice, we may need a finer temporal resolution of a signal component found in the prompt STFT output that has a coarse temporal resolution (but a fine spectral resolution), which is an application of the proposed technique in this subsection. Otherwise, new multiple STFTs with a smaller time window may be needed to be applied to the same sample data. In the following analysis, since the proposed backward STFT enhancement technique is applied to a prompt STFT output, we omit m_2 for algebraic simplicity.

To estimate the temporal information of $X_1[k_1, n_2]$ that has N_2 times finer temporal resolution than $X_2[k_2, m_2]$, we may start with N_1-point STFT of the input signal $x_1[n_1, n_2]$ expressed in terms of $X_2[k_2, m_2]$ as

$$X_1[k_1', n_2] = \sum_{n_1=0}^{N_1-1} x_1[n_1, n_2] e^{-j2\pi k_1' n_1/N_1} \tag{15a}$$

$$= \frac{1}{N_1N_2} \sum_{n_1=0}^{N_1-1} \sum_{k_1=0}^{N_1-1} \sum_{k_0=0}^{N_2-1} X_2[k_0 + N_2k_1] \times e^{(j2\pi k_0 n_1/(N_1N_2))} e^{j2\pi k_0 n_2/N_2} e^{j2\pi k_1' n_1/N_1} \times e^{-j2\pi k_1 n_1/N_1} \tag{15b}$$

$$= \frac{1}{N_2} \sum_{n_1=0}^{N_1-1} \sum_{k_0=0}^{N_2-1} X_2[n_1, k_0] \times e^{(j2\pi k_0 n_1/(N_1 N_2))} e^{j2\pi k_0 n_2/N_2} e^{-j2\pi k_1' n_1/N_1}, \tag{15c}$$

where k_1' is a new index that has the same dimension to k_1, and m_2 of $X_2[k_2, m_2]$ is dropped in (15b). Utilizing the multiplication-convolution duality property of the Fourier transform [17], (15c) can be expressed as

$$X_1[k_1', n_2] = \sum_{k_0=0}^{N_2-1} \left(X_2[k_1', k_0] \circledast H_{21}[k_1', k_0] \right) e^{j2\pi k_0 n_2/N_2}, \tag{16}$$

where

$$H_{21}[k_1', k_0] = \sum_{n_1=0}^{N_1-1} e^{(j2\pi k_0 n_1/(N_1 N_2))} e^{-j2\pi k_1' n_1/N_1} = \frac{1 - e^{j2\pi(k_0 - N_2 k_1)/N_2}}{1 - e^{j2\pi(k_0 - N_2 k_1)/(N_1 N_2)}}. \tag{17}$$

The expression (16) describes the proposed backward STFT enhancement technique and shows that $X_1[k_1', n_2]$, whose temporal resolution is finer than $X_2[k_2]$, can be obtained using $X_2[k_2]$. In (16), each column of $H_{21}[k_1', k_0]$ is column-wise circular convolved with the same column of $X_2[k_1', k_0]$ first, and then row-wise IFFT is applied to the circular convolution output to obtain $X_1[k_1', n_2]$.

To see the effect of $H_{21}[k_1', k_0]$ on evaluating $X_1[k_1', n_2]$, we compare the No-H_{21} method that computes (16) without the circular convolution with $H_{21}[k_1', k_0]$ (i.e., $H_{21}[k_1', k_0] = \delta[k_1', k_0]$ is assumed) to the proposed backward STFT enhancement technique (16). Schematic diagrams for the No-H_{21} method and the proposed backward STFT enhancement technique are shown in Fig. 6(a) and Fig. 6(b), respectively. In the No-H_{21} method, the input signal is N_1N_2-point FFT'd, and the system decides if higher temporal resolution is required. When higher temporal resolution is needed, N_1N_2-point FFT results are stored row-wise in an $[N_1 \times N_2]$ array buffer, and then a N_2-point row-wise IFFT is applied to the buffered data. Note that the N_1N_2-point FFT output is the same to the N_1N_2-point STFT output $X_2[k_2, m_2']$, where m_2' is the m_2 at which moment we need a higher temporal resolution of the spectral components of interest. In the proposed backward STFT enhancement technique, the input signal is N_1N_2-point FFT'd (i.e., N_1N_2-point STFT'd), and the system decides if a higher temporal resolution is required. When required, the system applies the algorithm (16) to $X_2[k_2, m_2']$ to obtain $X_{1,E}[k_1', n_2]$ which is the estimation of STFT output having a finer temporal resolution than $X_2[k_2, m_2']$.

The performance of the No-H_{21} method and the proposed backward STFT enhancement technique is compared for an example in Fig. 7. The magnitude response and the phase variation of $H_{21}[k_1', k_0]$ (17) is similar to those of $H_{12}[k_1, k_0]$ (12), so $H_{21}[k_1', k_0]$ is not shown in Fig. 7. The resulting estimates of $X_1[k_1', n_2]$ with the No-H_{21} method and with the proposed backward STFT enhancement technique are

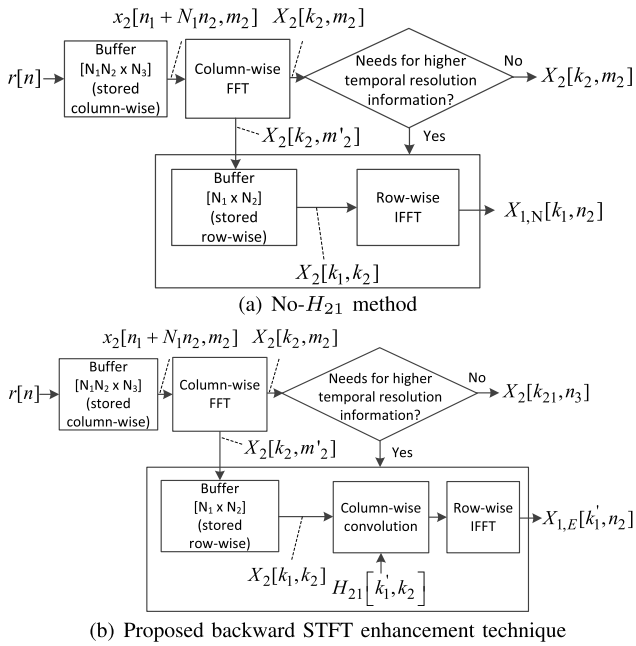

Fig. 6. Schematic diagrams of STFT methods for temporal resolution enhancement.

denoted as $X_{1,N}[k_1', n_2]$ and $X_{1,E}[k_1', n_2]$, respectively. In the simulation, we assume that $X_2[k_2, m_2']$ is obtained for a time window of $N_1N_2T_s = 1$ms during which three sinusoidal signals appear and disappear at different time instants. The three sinusoidal components are at $f_1 = -200$ kHz, $f_2 = 100$ kHz, and $f_3 = 300$ kHz, and the combined signal is sampled at $f_s = 1$ MHz (i.e., $T_s = 1\ \mu$s) and Fourier transformed to yield X_2 for $N_1 = 10$ and $N_2 = 100$ as shown in Fig. 7(a). The three signal components with frequency f_1 and f_3 appear at $n = 320$ (i.e., $n_1 = 20$, $n_2 = 30$) and disappear at $n = 760$ (i.e., $n_1 = 60$, $n_2 = 70$), respectively, and the signal with frequency f_2 exists during the whole time interval $N_1N_2T_s$. The 6 STFT outputs, out of 100 successive 10-point STFT outputs, with the same fixed time window of size N_1 are shown in Fig. 7(b). The magnitudes of the three frequency components with respect to the time index n_2 are shown in Fig. 7(c), which shows the appearance and disappearance of the signal components in the unit of 10 samples. The performance for the No-H_{21} method and the proposed backward STFT enhancement technique is shown in Fig. 7(d) and Fig. 7(e), respectively. As shown, the proposed backward STFT enhancement technique can obtain the correct temporal information without a noticeable error, while the No-H_{21} method may have a poor performance.

IV. Performance Analysis

In this section, we analyze the final approximation error in $X_2[k_2, m_2]$ caused by using the approximation of $H_{12}[k_1, k_0]$ in the proposed forward STFT enhancement technique. Note that the proposed backward STFT enhancement technique does not have a final approximation error, since the transform function $H_{21}[k_1', k_0]$ is not approximated. In addition, we provide algebraic comparison of computational complexities between the conventional STFT, No-H_{12} and No-H_{21} methods, and the proposed forward and backward STFT enhancement techniques.

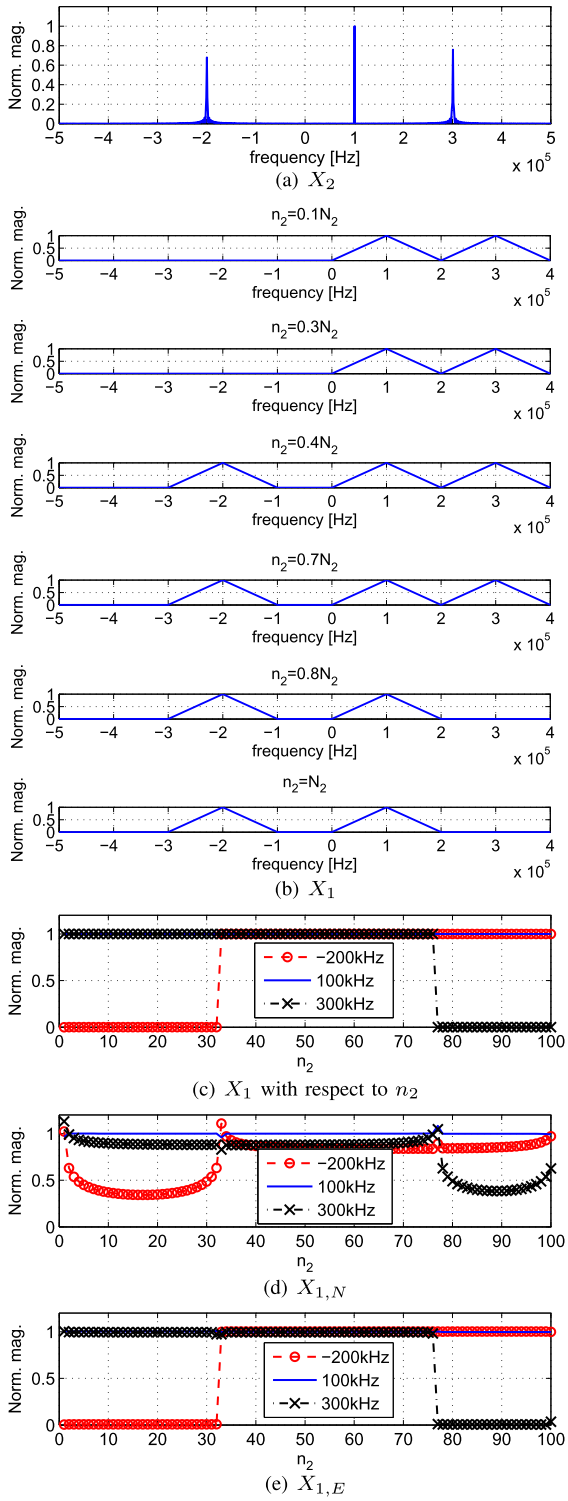

Fig. 7. Example of X_1 obtained from X_2.

A. Error Analysis

The estimation error caused by using the approximation of $H_{12}[k_1, k_0]$ in the proposed forward STFT enhancement technique is expressed as

$$E_2[k_1,k_0] = \sum_{n_2=0}^{N_2-1} \Big(X_1[k_1,m_1] \circledast H_{12}[k_1,\tilde{k}_{0,i}] - X_1[k_1,m_1] \circledast H_{12}[k_1,k_0] \Big) e^{-j2\pi k_0 n_2/N_2}. \quad (18)$$

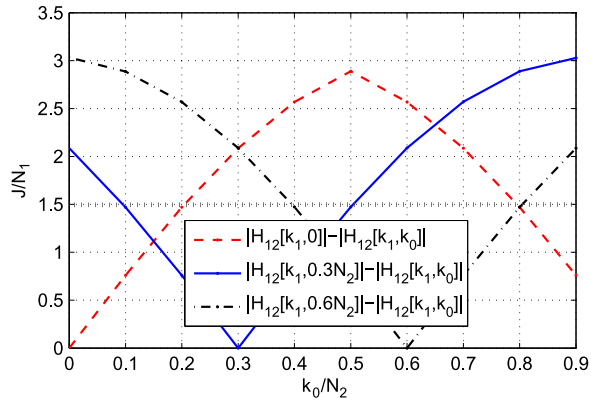

Fig. 8. J with respect to k_0 for $\beta = 0.3$.

Since the computation of $E_2[k_1, k_0]$ (18) is complicated because of the exponential term, we perform the error analysis in the time-domain, i.e., before applying the Fourier transform. We denote the equivalent error before the Fourier transform in (8c) as $e_2[k_0]$, then it is found that

$$e_2[k_0] = X_1[k_1,m_1] \circledast \Big(H_{12}[k_1,\tilde{k}_{0,i}] - H_{12}[k_1,k_0] \Big). \quad (19)$$

Let $X_1[k_1, m_1]$ be a bounded signal, then $|X_1[k_1, m_1]| < U_1$ for all k_1 and m_1, where U_1 is the finite upper bound on the magnitude of $X_1[k_1, m_1]$. Then the magnitude of $e_2[k_0]$ is bounded as

$$\begin{aligned} |e_2[k_0]| &= \Bigg| \sum_{m=-\infty}^{\infty} X_1[k_1-m,m_1] \times \Big(H_{12}[m,\tilde{k}_{0,i}] - H_{12}[m,k_0] \Big) \Bigg| && (20a) \\ &< \sum_{m=-\infty}^{\infty} |X_1[k_1-m,m_1]| \times \Big| H_{12}[m,\tilde{k}_{0,i}] - H_{12}[m,k_0] \Big| && (20b) \\ &< JU_1, && (20c) \end{aligned}$$

using the Cauchy-Schwarz inequality principle, where

$$\begin{aligned} J &= \sum_{k_1=0}^{N_1-1} \Big| H_{12}[k_1,\tilde{k}_{0,i}] - H_{12}[k_1,k_0] \Big| \\ &= \sum_{k_1=0}^{N_1-1} \Bigg| \frac{1-e^{-j2\pi\tilde{k}_{0,i}/N_2}}{1-e^{-j2\pi(\tilde{k}_{0,i}+N_2k_1)/(N_1N_2)}} - \frac{1-e^{-j2\pi k_0/N_2}}{1-e^{-j2\pi(k_0+N_2k_1)/(N_1N_2)}} \Bigg|, \end{aligned} \quad (21)$$

In the following simulations, $\beta = 0.3$ is used as an appropriate value to reduce the computational complexity and the approximation error of the proposed technique. As shown in Fig. 8, it is found that J is lower than $1.5N_1$.

B. Computational Complexity

In this subsection, the computational complexity of the proposed techniques is compared to the conventional STFT and the No-H_{12} and No-H_{21} methods, where the computational complexity represents the number of required complex multiplications. In the forward processing of the conventional STFT, i.e.,

from $x_1[n_1, m_1]$ to $X_2[k_2, m_2]$ in Fig. 2(a), the computational complexity is found as

$$\Omega_{12,C} = N_2 N_1 \log_2 N_1 + N_1 N_2 \log_2(N_1 N_2). \quad (22)$$

In the conventional STFT, N_2 times of N_1-point STFT are performed first, and an $N_1 N_2$-point FFT is performed to obtain N_2 times finer spectral information.

In the No-H_{12} method, N_2 times of N_1-point STFT is computed first, and row-wise FFT's are applied to the frequency components of interests, where we assume that the frequency range of $1/T_s/N_1$ wide around the frequency of the target signal is successfully determined. The computational complexity required to obtain $X_{2,N}[k_2, m_2]$ from $x_1[n_1, m_1]$ in Fig. 4(a) is

$$\Omega_{12,N} = N_2 N_1 \log_2 N_1 + N_r N_2 \log_2(N_2), \quad (23)$$

where N_r is the number of frequency ranges of interests.

In the proposed forward STFT enhancement technique, N_2 times of N_1-point STFT are performed first, and the circular convolution with the approximated $H_{12}[k_1, k_0]$ in (12) and an FFT are performed to estimate spectral information with N_2 times higher precision. The overall computational complexity to obtain $X_{2,E}[k_2, m_2]$ from $x_1[n_1, m_1]$ in Fig. 4(b), is found as

$$\Omega_{12,E} = N_2 N_1 \log_2 N_1 + N_r N_2 \log_2 N_2 + \left\lfloor \frac{1}{\beta} \right\rfloor (N_1 N_2 + N_r N_2 \log N_2). \quad (24)$$

In the case of backward processing of the conventional STFT, $N_1 N_2$-point STFT is computed first, and N_1-point STFT is computed N_2 times to search for the temporal information with higher precision, which corresponds to the operations to obtain $X_1[k_1, m_1]$ from $x_2[n_1 + N_1 n_2, m_2]$ in Fig. 2(b). Therefore, the computational complexity for the conventional STFT is found as

$$\Omega_{21,C} = N_2 N_1 \log_2(N_2 N_1) + N_2 N_1 \log_2 N_1. \quad (25)$$

In the No-H_{21} method, $N_1 N_2$-point STFT is executed first, and a row-wise IFFT is applied to the temporal range of interests, which is from $x_2[n_1 + N_1 n_2, m_2]$ to $X_{1,N}[k_1, n_2]$ in Fig. 6(a). Therefore, the computational complexity for the No-H_{21} method is as

$$\Omega_{21,N} = N_2 N_1 \log_2(N_2 N_1) + N_r N_2 \log_2 N_2. \quad (26)$$

In the proposed backward STFT enhancement technique, $N_1 N_2$-point STFT is performed first, and the circular convolution with $H_{21}[k_1', k_0]$ in (17) and IFFT operation are used to achieve N_2 times finer temporal resolution. The computational complexity required from $x_2[n_1 + N_1 n_2, m_2]$ to $X_{1,E}[k_1, n_2]$ in Fig. 6(b) is found as

$$\Omega_{21,E} = N_2 N_1 \log_2(N_2 N_1) + N_r N_1 N_2 + N_r N_2 \log_2 N_2. \quad (27)$$

The analysis in this section is to find the computational complexity of the techniques in terms of the number of required complex multiplications. In the next section, we compare the performance of the techniques with respect to N_1, N_2, and β.

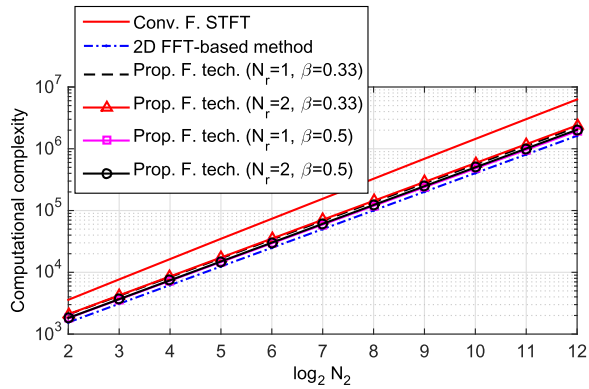

Fig. 9. Computational complexity for spectral resolution enhancements with $N_1 = 64$.

V. Numerical Results

In this section, the computational complexity of the proposed technique is compared with the conventional STFT techniques with simulations. The computational complexity is compared in terms of various values of N_1, N_2, and β. The sampling frequency used is $f_s = 1$ MHz.

Fig. 9 shows the computational complexity of the forward STFT enhancement technique $\Omega_{12,E}$ (denoted as 'Prop. F. Tech.' in the figure) for $N_1 = 64$. In this simulation, the computational complexity is compared to those of the conventional technique $\Omega_{12,C}$ (denoted as 'Conv. F. STFT') described in Fig. 1 and the No-H_{12} method $\Omega_{12,N}$ described in Fig. 4(a). As shown, the computational complexity of the proposed forward STFT enhancement technique is $2 \sim 5$ times less than that of the conventional STFT technique, but the No-H_{12} method has similar complexity to the proposed technique; however, the final error $|X_2 - X_{2,N}|$ of the No-H_{12} method is much larger than $|X_2 - X_{2,E}|$ of the proposed technique as expected from Section IV. As N_2 increases, the computational savings with the proposed technique over the conventional technique increases. In other words, when the higher spectral resolution is required, larger computational cost reduction with the proposed technique than the conventional technique can be obtained. As N_r increases, the computational complexity increases as expected. Also as β decreases, $|X_2 - X_{2,E}|$ which is related to (12) decreases; however, the computational complexity increases.

Fig. 10 shows the computational complexity of the backward STFT enhancement technique $\Omega_{21,E}$ (denoted as 'Prop. B. Tech.' in the figure) for $N_1 = 64$ compared to those of the conventional technique $\Omega_{21,C}$ (denoted as 'Conv. B. STFT') in Fig. 1 and No-H_{21} method $\Omega_{21,N}$ in Fig. 4(a). The computational complexity of the proposed backward STFT enhancement technique is $1 \sim 2$ times less than that of the conventional STFT technique, but the No-H_{12} method has a similar complexity to the proposed technique; however, $|X_1 - X_{1,N}|$ is much larger than $|X_1 - X_{1,E}|$ as discussed in Section IV. As N_2 decreases, the advantage of the proposed technique over the conventional technique increases. Therefore, the higher temporal resolution is required, the more advantage the proposed technique is achievable over the conventional technique. In addition, as N_r increases, the computational complexity increases as expected.

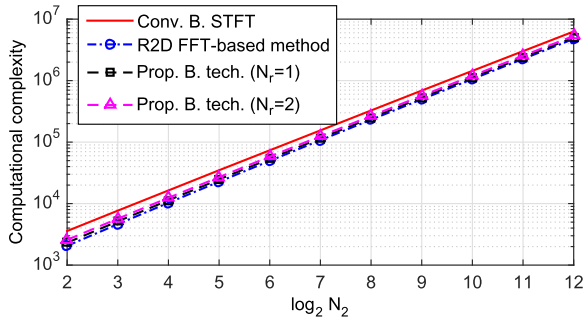

Fig. 10. Computational complexity for temporal resolution enhancements with $N_1 = 64$.

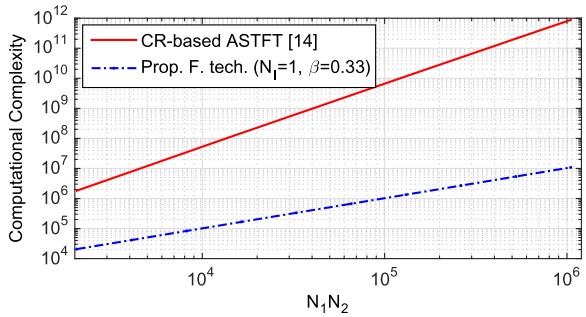

Fig. 11. Computational complexity of forward STFT enhancement technique comparing to ASTFT.

To demonstrate the performance of the proposed techniques in the radar ranging applications using linear chirp signals, the computational complexity of the forward STFT enhancement technique is compared to that of the CR-based ASTFT [14]. Fig. 11 shows the computational complexity for the estimation of the time difference between the transmitted chirp signal and the received chirp signal. The estimation process for the time difference is different for the forward STFT enhancement technique and the CR-based ASTFT; In the forward STFT enhancement technique, the received chirp signal is first de-chirped and the frequency of the obtained continuous-wave (CW) signals is estimated to find the time difference. In the CR-based ASTFT, the linear chirp signal is analyzed using wavelet transform (WT), from which an appropriate STFT time window size is determined. Then the conventional STFT with the estimated time window size is performed to estimate the spectral information of the received chirp signal. The instantaneous frequency is computed every 10 samples in the CR-based ASTFT, and $N_1 = 128$ in the forward STFT enhancement technique. Due to the heavy computational cost for the WT, computational complexity of the CR-based ASTFT for the linear chirp signal is much larger than that of the forward STFT enhancement technique. In addition, as the total number of samples increases, the proposed technique has larger advantage than the CR-based ASTFT.

To test the SNR degradation due to the estimation error $E_2[k_1, k_0]$ (18), SNR of $X_2[k_2, m_2]$ and $X_{2,E}[k_2, m_2]$ is compare when $r[n]$ is from a single tone CW input signal samples and the SNR of $r[n]$ ranges from -20 dB to 20 dB. In this simulations, we use $N_1 = 10$ and $N_2 = 100$. As shown in Fig. 12, when SNR is below about 10 dB, there is a small SNR difference between $X_2[k_2, m_2]$ and $X_{2,E}[k_2, m_2]$, however, the SNR difference keeps increasing as the SNR of the input

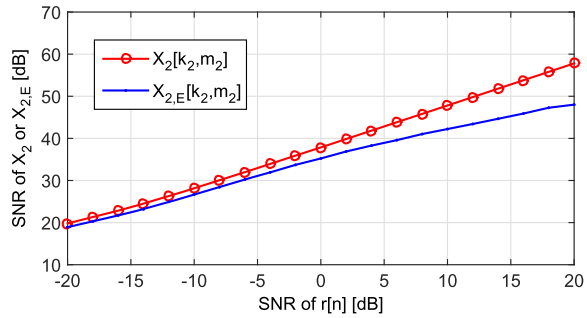

Fig. 12. SNR of forward STFT enhancement technique.

signal increases over 10 dB, which is because as the input SNR increases, the magnitude difference between the unwanted side peaks caused by the approximation shown in Fig. 5(e) and noise terms increases. However, the goal of the proposed technique is to enhance the spectral and temporal resolution of a detected signal rather than to increase the detection sensitivity. Therefore, the SNR degradation shown in Fig. 12 would not be a critical problem in enhancing the spectral and temporal resolution using the proposed techniques.

VI. Conclusion

In this paper, two low computational enhanced STFT-based spectral and temporal estimation techniques for radar signal processing have been proposed. The forward STFT enhancement technique uses consecutive STFT outputs, having a coarse spectral resolution, to estimate precise spectral information of the original signal. And the backward STFT enhancement technique uses an STFT output, having a poor temporal resolution due to the wide time window, to obtain accurate temporal information of the appearance and disappearance of the target signal within the wide time window. The proposed forward and backward STFT enhancement techniques require 2 $\sim$ 5 and 1 $\sim$ 2 times less computational complexity than the conventional STFT technique, respectively. The proposed low computational enhanced STFT-based parameter estimation techniques can be useful for low cost real-time radar signal processor that performs the time-frequency analysis.

References

[1] S. G. Mallat, *A Wavelet Tour of Signal Processing*. New York, NY, USA: Academic, 1998.
[2] D. L. Johns and R. G. Baraniuk, "An adaptive optimal-kernel time-frequency representation," *IEEE Trans. Signal Process.*, vol. 43, no. 10, pp. 2361–2371, Oct. 1995.
[3] D. Gabor, "Theory of communications," *J. IEE*, vol. 93, no. 3, pp. 429–457, 1946.
[4] B. Boashash and G. Frazer, "Time varying higher order spectra, generalized Wigner-Ville distributions, and the analysis of underwater acoustic data," in *Proc. IEEE ICASSP*, San Francisco, CA, USA, Mar. 1992.
[5] B. Boashash and P. J. Black, "An efficient real-time implementation of the Wigner-Ville distribution," *IEEE Trans. Acoust., Speech, Signal Process.*, vol. ASSP-35, pp. 1611–1618, Nov. 1987.
[6] J. Xiam and P. Flandrin, "Multitaper time-frequency reassignment for nonstationary spectrum estimation and chirp enhancement," *IEEE Trans. Signal Process.*, vol. 55, no. 6, pp. 2851–2860, May 2007.
[7] E. Sejdic, I. Djurovic, and J. Jiang, "Time-frequency feature representation using energy concentration: An overview of recent advances," *Dig. Signal Process.*, vol. 19, no. 1, pp. 153–183, Jan. 2009.

[8] F. Jaillet and B. Torresani, "Time-frequency jigsaw puzzle: Adaptive multiwindow and multilayered Gabor expansions," *Int. J. Wavelets Multiresolut. Inf. Process.*, vol. 5, no. 2, pp. 293–315, Mar. 2007.
[9] D. Rudoy, P. Basu, T. F. Quatieri, B. Dunn, and P. J. Wolfe, "Adaptive short-time analysis-synthesis for speech enhancement," in *Proc. IEEE ICASSP*, Las Vegas, NV, USA, Mar. 2008.
[10] S. M. Qaisar, L. Fesquet, and M. Renaudin, "An adaptive resolution computationally efficient short-time Fourier transform," *Res. Lett. Signal Process.*, vol. 2008, p. 10.
[11] Y. Jiang and Y. He, "Frequency estimation of electric signals based on the adaptive short-time Fourier transform," *Int. J. Electron.*, vol. 96, no. 3, pp. 267–279, 2009.
[12] D. L. Jones and T. W. Parks, "A high resolution data-adaptive time-frequency representation," *IEEE Trans. Acoust., Speech, Signal Process.*, vol. 38, no. 12, pp. 2127–2135, Dec. 1990.
[13] S. C. Pei and P. W. Wang, "Energy concentration enhancement using window width optimization in s transform," in *Proc. IEEE ICASSP*, Dallas, TX, USA, Mar. 2010, pp. 4106–4109.
[14] J. Zhong and Y. Huang, "Time-frequency representation based on an adaptive short-time Fourier transform," *IEEE Trans. Signal Process.*, vol. 58, no. 10, pp. 5118–5128, Oct. 2010.
[15] S.-C. Pei and S.-G. Huang, "STFT with adaptive window width based on the chirp rate," *IEEE Trans. Signal Process.*, vol. 60, no. 8, pp. 4065–4080, Aug. 2012.
[16] A. V. Oppenheim, R. W. Schafer, and J. R. Buck, *Discrete-Time Signal Processing*, 2nd ed. Upper Saddle River, NJ: Prentice-Hall, 1999.
[17] M. J. Roberts, *Fundamentals of Signals and Systems*. New York, NY, USA: McGraw-Hill Science/Engineering/Math, 2007.

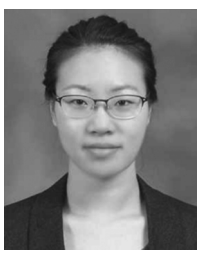

Binhee Kim (M'15) received B.S. and M.S. degrees in electrical engineering from the Korea Advanced Institute of Science and Technology (KAIST), Daejeon, Korea, in 2008 and 2010, respectively. She is a Researcher in the CCS Graduate School for Green Transportation at KAIST, where she received a Ph.D. degree in 2015. Her research interests include radar signal processing, GNSS signal processing, and detection and estimation for navigation systems.

Seung-Hyun Kong (M'06) received a B.S.E.E. from Sogang University, Korea, in 1992, an M.S.E.E. from Polytechnic University, New York, in 1994, and a Ph.D. degree in aeronautics and astronautics from Stanford University, CA, in 2006. From 1997 to 2004, he was with Samsung Electronics Inc. and Nexpilot Inc., both in Korea, where his research focus was on 2G CDMA and 3G UMTS PHY and mobile positioning technologies. In 2006, he was involved with hybrid positioning technology development using wireless location signature and Assisted GNSS at Polaris Wireless, Inc. and from 2007 to 2009, he was a Research Staff at Qualcomm Research Center, San Diego, CA, where his R&D focused on indoor location technologies and advanced GNSS technologies. Since 2010, he has been an Assistant Professor at the Department of Aerospace Engineering in the Korea Advanced Institute of Science and Technology (KAIST). His research interests include super-resolution signal processing, detection and estimation for navigation systems, and assisted GNSS in wireless communication systems.

Suil Kim He was born in Jejudo, Korea, in 1964. He received the B.S. and M.S. degrees in electrical engineering from Soongsil University, Seoul, Korea in 1986 and 1988, respectively, and Ph.D. degree in electrical engineering & computer science from Korea Advanced Institute of Science and Technology (KAIST), Daejeon, Korea, in 2000. Since 1988, he has been with Agency for Defense Development (ADD) in Daejeon, Korea and continues to work in the area of military tactical satellite/mobile/wireless communications and networks. Currently, he is a principal researcher/project manager in ADD and a professor in the University of Science and Technology (UST) in Daejeon, Korea. His research interests include the anti-jamming modems, interference cancellation for military satellite and mobile wireless communication systems under jamming environment. He also has interests in networking technology under Network Centric Operation Environment (NCOE).